NANO LETTERS

pubs.acs.org/NanoLett Letter

Anodic TiO_2 Nanotubes on 3D-Printed Titanium Meshes for Photocatalytic Applications

Hanna Sopha, Adelia Kashimbetova, Ludek Hromadko, Ivan Saldan, Ladislav Celko, Edgar B. Montufar, and Jan M. Macak*

Cite This: *Nano Lett.* 2021, 21, 8701−8706 Read Online

ACCESS | Metrics & More | Article Recommendations | Supporting Information

ABSTRACT: In this work, large 3D Ti meshes fabricated by direct ink writing were wirelessly anodized for the first time to prepare highly photocatalytically active TiO_2 nanotube (TNT) layers. The use of bipolar electrochemistry enabled the fabrication of TNT layers within the 3D Ti meshes without the establishment of an electrical contact between Ti meshes and the potentiostat, confirming its unique ability and advantage for the synthesis of anodic structures on metallic substrates with a complex geometry. TNT layers with nanotube diameters of up to 110 nm and thicknesses of up to 3.3 μm were formed. The TNT-layer-modified 3D Ti meshes showed a superior performance for the photocatalytic degradation of methylene blue in comparison to TiO_2-nanoparticle-decorated and nonanodized Ti meshes (with a thermal oxide layer), resulting in multiple increases in the dye degradation rate. The results presented here open new horizons for the employment of anodized 3D Ti meshes in various flow-through (photo)catalytic reactors.

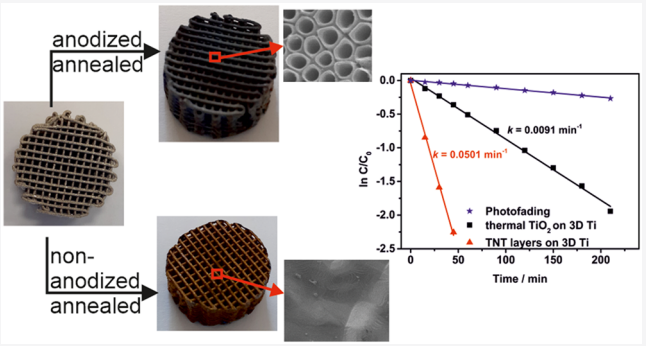

KEYWORDS: *TiO_2 nanotube layers, bipolar electrochemistry, 3D Ti mesh, 3D printing, direct ink writing, photocatalysis*

One-dimensional TiO_2 nanostructures have gained tremendous attention in the last decades due to their intriguing applications as sensors, solar cells, and photocatalysts.[1,2] Among the different nanostructures, anodic TiO_2 nanotube (TNT) layers are highly ordered, are strongly light absorbing, and are directly connected to a Ti substrate that can act as a back contact. Furthermore, anodic TNT layers are easy to prepare, using low-cost instrumentation, with well-controllable dimensions, such as the nanotube diameter and layer thickness, and possess a high surface to volume ratio.[1,2] Flat Ti substrates, such as foils and sheets, are most frequently used for TNT layer production. However, within the past decade several works have been dedicated to the anodization of more complex Ti substrates, including 2D meshes,[3−5] wires,[6−8] and spheres,[9] with the aim of maximizing the surface coated with TNT layers, which is of paramount importance for catalytic, sensing, and solar conversion applications.

Additive manufacturing opens the door to the fabrication of near-net-shaped, self-supported, three-dimensional (3D) substrates with a regular and periodic porous network that maximizes the surface for the anodic growth of TNT layers, allows the homogeneous flow of fluids, minimizes the dead volume of the catalytic reactor, and avoids pressure drops, especially in the flow-through arrangement. Such open-cell porous Ti meshes, further denoted as 3D Ti meshes, can be fabricated by direct ink writing (DIW), a method based on the computer-controlled extrusion of a Ti paste (ink) following a predesigned *in silico* pattern and sintering of the deposited part.[10] DIW, also known as robocasting, can produce periodic 3D meshes with different pore architectures by changing the path that the extrusion robot follows for ink deposition. The pore size is controlled by setting the distance between the deposited filaments. The height of the 3D mesh depends on the number of layers stacked, and the filament diameter depends on the aperture of the nozzle used for extrusion. Unlike other metal additive manufacturing technologies based on powder bed fusion, such as selective laser melting and electron beam melting, DIW only uses the amount of powder needed for the fabrication of the mesh,[10] reducing operation costs and waste of the material.

The challenge is the anodization of 3D Ti meshes with a relevant size for the production of efficient (photo)catalytic reactors, due to the high surface area and the high possibility of dielectric breakdown during anodization.[11] Only recently have TNT layers been produced by two-step anodization of

Received: July 20, 2021
Revised: October 1, 2021
Published: October 5, 2021

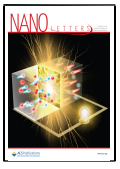

https://doi.org/10.1021/acs.nanolett.1c02815
Nano Lett. 2021, 21, 8701−8706

relatively small 3D titanium alloy porous 3D meshes to enhance osseointegration.[12] While the size of the 3D Ti-6Al-4V porous meshes (d = 10 mm and h = 2 mm) fabricated by selective laser melting was sufficient enough for cell culture growth on the laboratory scale, it is too small for any reasonable catalytic application. Apart from that work, the anodization of additive manufactured structures made of Ti and Ti alloys has been reported only for solid plates, strips, sheets, bars, conical arrays, and two-dimensional meshes,[13−21] but never for 3D meshes. Furthermore, these anodized-Ti-based structures were only used for biomedical applications[12−20] and water splitting[21] but never for (photo)catalytic applications.

While they have been commonly produced by anodic oxidation using the Ti substrate as the anode, it was recently shown that TNT layers can be produced wirelessly as well by employing bipolar electrochemistry.[9,22−27] The advantage of this approach is that the Ti substrate does not need to be directly connected to the potentiostat. Thus, especially small metal objects or complicated metallic shapes, such as the 3D shapes shown here, can be anodized. It is also possible to anodize the complete Ti substrate without establishing any electrical contact,[9] which could release unwanted ions to the electrolyte, if it is made from a material other than Ti, and thus poison the electrolyte. Furthermore, a cut of the electric contact due to dielectric breakdown when high-surface-area Ti substrates are anodized is avoided using wireless bipolar electrochemistry.[11] These unique features are of paramount importance to allow the anodization of complicated 3D Ti shapes and to exploit some new advanced applications of TNT layers.

In the present work, the wireless anodization of 3D Ti meshes with two different filament spacings produced by DIW is demonstrated for the first time by employing bipolar electrochemistry, using the anodization setup shown in Figure 1a. The 3D Ti mesh was placed between two Pt foils (feeder electrodes), which were connected to the potentiostat. Each

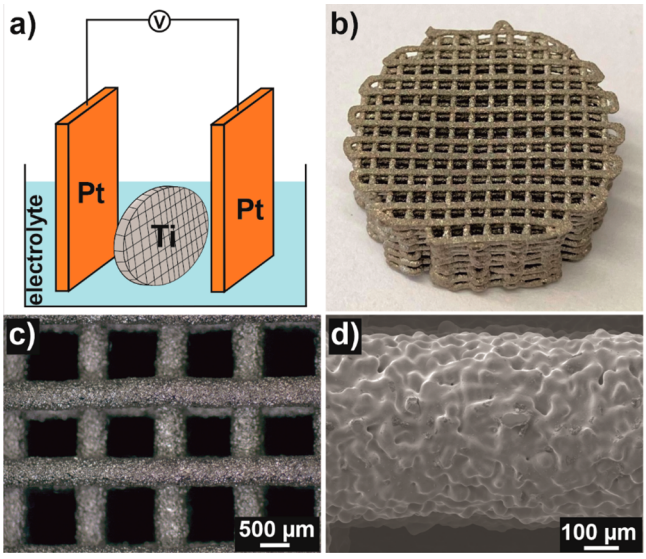

Figure 1. (a) Scheme of the anodization setup based on bipolar electrochemistry. (b) Photograph of the cylindrical 3D Ti mesh with a filament spacing of ∼857 μm as fabricated by DIW. (c, d) SEM images of the filaments of nonanodized Ti meshes with a filament spacing of ∼857 μm.

3D Ti mesh had a diameter of 20 mm and a height of 8 mm and consisted of an orthogonal Cartesian grid pattern (Figure 1b,c), allowing the flow of gases and liquids. This is an advantage in the case of fluid-phase catalysis and photocatalysis, as the whole surface of the meshes will be in contact with the reacting molecules of the fluid. Exact details on the effective surface area and porosity of the meshes can be found in Methods. In fact, the surface area and the porosity can be tuned by computer-aided design to promote the interaction with the fluid and the fluid flow through the mesh. The filaments forming the meshes showed sintered Ti particles that result in an uneven surface (Figure 1d). The roughness of the Ti substrate is known to influence the ordering of the nanotubes;[28,29] however, in general TNT layers grow on Ti substrates with rough as well as smooth surfaces. Thus, it is expected that the roughness of the 3D Ti meshes does not influence the overall TNT layer growth.

In order to anodize the 3D porous Ti meshes in a fluoride ion containing ethylene glycol based electrolyte, an alternating potential with an amplitude of 140 V and frequency of 0.0667, 0.0167, or 5.55×10^{-4} Hz was applied, meaning the potential was changed every 15 s, 60 s, or 30 min, respectively. The applied potential was selected by considering two factors. First, the potential should be high enough to prepare TNT layers on the whole sample:[9] i.e., on the filaments close to the edge and also in the filaments in the middle of the meshes. Second, to prevent dielectric breakdown events, the current flowing between the feeder electrodes should not heat up the electrolyte above room temperature.[30,31] At a potential of 140 V currents of up to 500 mA were reached and the electrolyte temperature increased significantly during the anodization process, even though the electrolyte was precooled to 5 °C before anodization and a cooling system was employed during the process, limiting the potential to this amplitude. It must be emphasized here that, even though the anodized surface area and consequently the recorded currents were extremely high, no sign of dielectric breakdown was observed. Thus, the use of bipolar electrochemistry gives a possibility to anodize large surface areas, reducing the otherwise very high risk of dielectric breakdown.

Figure 2a shows that TNT layers were successfully produced within the 3D meshes. As expected, the uneven surface of the Ti filaments (Figure 1d) did not influence the overall TNT layer growth. As shown in Figure 2b, the average diameters of the nanotubes received by applying the mentioned different frequencies were relatively similar to 111.6 ± 9.7, 80.9 ± 10.6, and 78.9 ± 10.4 nm, respectively. SEM images were taken of both upper sides of the 3D Ti meshes, and the measured diameters were in the same range on both sides. In terms of the nanotube dimensions inside the 3D mesh, one can state that on the basis of a preliminary investigation of the nanotube layers inside the mesh (upon cutting and SEM observation), average diameters and layer thicknesses were about ∼30−40% smaller (not shown here) in the middle of the meshes than at the sides facing the feeder electrodes directly. This is due to an unequal distribution of the potential along the 3D Ti meshes, when bipolar electrochemistry is used for anodization.[9,23]

The frequency had a large effect on the average thickness of the TNT layers, which was around 1.7 times thicker at low frequency (3.3 ± 0.7 μm for 5.55×10^{-4} Hz) than at higher frequencies (1.86 ± 0.8 and 1.95 ± 0.2 μm for 0.0667 and 0.0167 Hz, respectively). The growth of the nanotubes was limited at higher frequencies, because for each alternation of

https://doi.org/10.1021/acs.nanolett.1c02815
Nano Lett. 2021, 21, 8701−8706

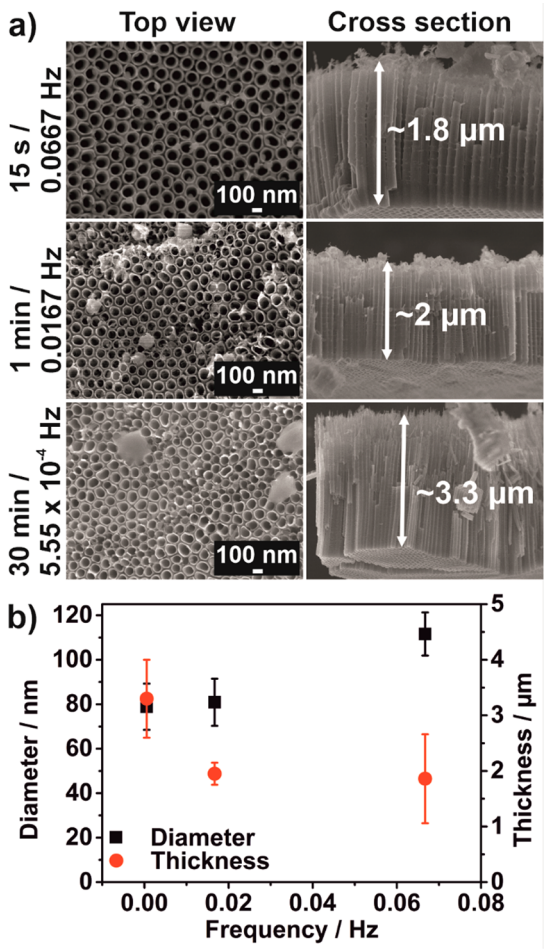

Figure 2. (a) SEM images of TNT layers produced on 3D Ti meshes with filament spacing of ~857 μm using alternating potentials of different frequencies. The times given on the left side correspond to the anodization time before the direction of the potential was changed. (b) Diagram showing the dependence of nanotube diameter and TNT layer thickness on the frequency of the applied alternating potential. The error bars indicate the standard deviation.

the potential a new electrochemical equilibrium has to be established, reducing the time for the thickening of the layer. The relatively large standard deviation for the TNT layer thicknesses is related to the strong influence of the layer thickness on the anodization potential, which varies along the 3D Ti mesh.[9,23] Even along one Ti filament (one wire of the 3D Ti mesh) the applied potential varies, with the highest potential on the side of the filament facing the feeder electrode.

Figure 3a shows X-ray diffraction (XRD) patterns of 3D Ti meshes that were anodized and annealed and 3D Ti meshes that were nonanodized but annealed: i.e., with a thermal oxide layer. Figure 3b shows the patterns for classical Ti foils prepared in a conventional anodization setup as reference. TNT layers on 3D Ti meshes and foils consisted of the anatase phase with the main peak at 2θ = 25.4° corresponding to the (101) orientation (ICDD: 00-021-1272). The visible Ti signals (ICDD: 04-005-7594) stem from the underlying Ti substrates. Intensities recorded for the 3D Ti meshes (Figure 3a) were much lower than for the Ti foils (Figure 3b) due to the porosity of the meshes, which reduces the area analyzed by the X-rays. Thus, in general, no differences between the main anatase phases were recorded for the anodized Ti foil and 3D Ti mesh. In contrast, with a thermal oxide layer there was no signal of TiO_2, as the oxide layer was very thin, and the X-rays penetrated through it. Grazing incident XRD was not used to reduce the penetration depth, as the morphology of the 3D Ti meshes forbids this. However, after annealing a color change of the 3D Ti meshes and foils was visible, indicating the formation of thermal TiO_2.

3D Ti meshes with two different filament spacings (857 and 1173 μm) were anodized by applying a frequency of 5.55×10^{-4} Hz to obtain thick TNT layers. Afterward, they were employed for the photocatalytic degradation of methylene blue (MB) dye, as a model pollutant. Ti meshes decorated with TiO_2 nanoparticles (NPs) and nonanodized annealed Ti meshes with a thermal oxide layer were used as reference. SEM images of the NP-decorated Ti meshes are shown in Figure S1.

Figure 4a shows the photocatalytic experimental setup, with six Ti meshes stacked in a closed quartz-glass reactor together with a magnetic stirring bar. The photocatalytic degradation rates of MB are shown in Figure 4b. The degradation rate constants were calculated to be k = 0.0501, 0.0288, and 0.0091 min^{-1} for the anodized, NP-decorated and nonanodized annealed 3D Ti meshes with 857 μm spacing and k = 0.0219, 0.0132, and 0.0089 min^{-1} for the anodized, NP decorated and nonanodized annealed 3D Ti meshes with 1173 μm spacing, respectively. The approximately 5.5 times enhancement of the rate constant for the anodized Ti meshes

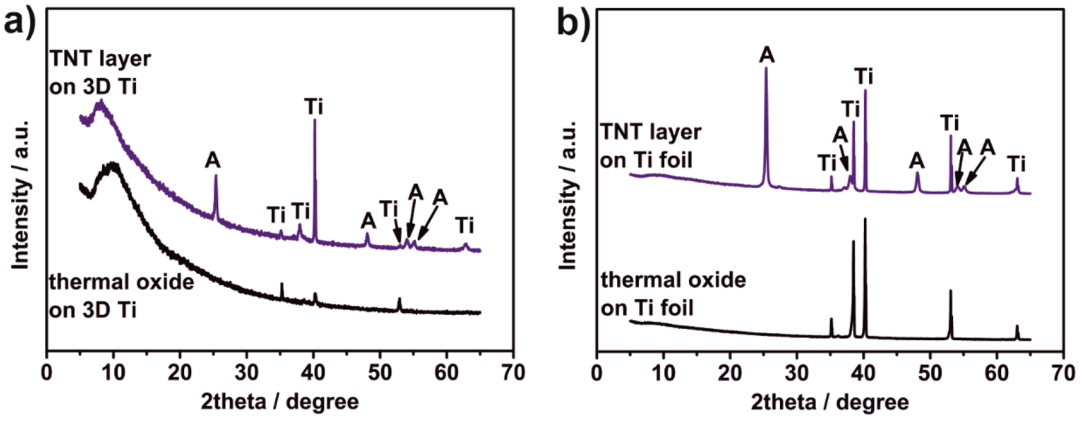

Figure 3. XRD patterns of the anodized annealed and nonanodized annealed (a) 3D Ti meshes (filament spacing 857 μm) and (b) classical Ti foils. Abbreviations: A, anatase; Ti, α-titanium.

https://doi.org/10.1021/acs.nanolett.1c02815
Nano Lett. 2021, 21, 8701−8706

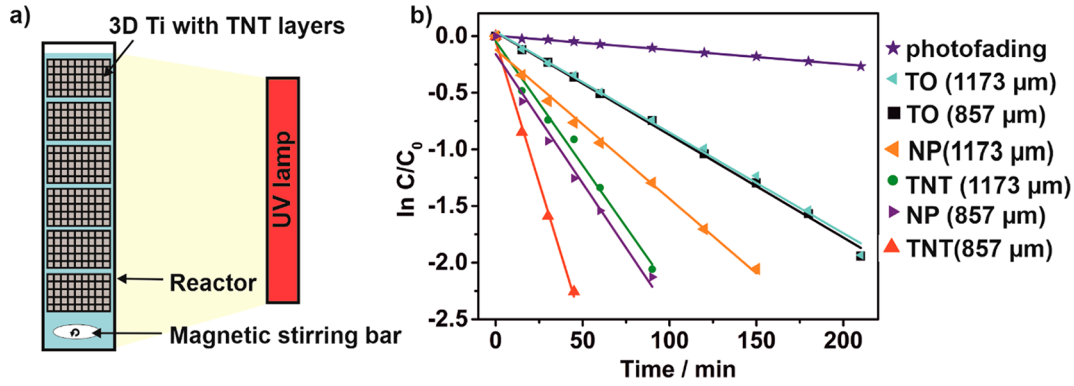

Figure 4. (a) Scheme of the setup used for the photocatalytic degradation of MB. (b) Photocatalytic degradation kinetics of MB on anodized annealed (TNT), NP-decorated annealed (NP), and nonanodized annealed 3D Ti meshes (TO) with filament spacings of 857 and 1173 μm. Photofading describes the degradation of MB upon UV light illumination in the absence of a catalyst.

with 857 μm filament spacing and approximately 2.4 times enhancement of the rate constant for the anodized Ti meshes with 1173 μm filament spacing in comparison to the nonanodized annealed Ti meshes was attributed to the significantly increased available TiO_2 active surface area of the anodized Ti meshes. In the case of the NP-decorated Ti meshes, there were 3.2 times and 1.5 times enhancements for meshes with 857 and 1173 μm filament spacing, respectively, in comparison to the nonanodized annealed Ti meshes. Clearly, the performance of the NP-decorated Ti meshes was lower than that for the anodized Ti meshes with TNT layers. This difference is attributed to the fact that only the uppermost part of the NP layer is active, even though the light is absorbed sufficiently deep in the layers. On the other hand, for the anodized Ti meshes with TNT layers, the photocatalytic reactants and products can reach the interiors of the nanotubes, which are also strongly light absorbing. Thus, there is a greater surface area available for the light-driven photocatalytic reaction.

Figure S2 shows SEM images of the TNT layers on 3D Ti meshes after the photocatalytic experiments. As one can see, the TNT layers do not show any defects that would stem from the photocatalytic experiment. The SEM images of the NP-decorated Ti meshes after photocatalytic experiments are shown in Figure S3. Also, in this case, hardly any changes are visible in comparison to the unused Ti meshes. This demonstrates the usability and robustness of the anodized high-surface-area 3D Ti meshes in photocatalysis and, in principle, in any catalytic reaction, where TiO_2 can act as a catalyst or catalyst support.

In comparison to a reactor packed with spheres (beads) it should be easier for the liquid to flow through the 3D meshes (essentially regardless of composition or surface chemistry). With packaged spheres a higher pressure would probably be needed to maintain the flow at the same speed. Furthermore, the mechanical strength of the 3D Ti meshes provides structural support to the catalytic reactor and the pattern of the meshes can be optimized to maximize the active surface area, while allowing fluid flow through the whole structure without significant fluid flow reduction. The structural optimization of the 3D Ti meshes is in fact a topic for future research, together with the exploration of different anodization and pretreatment conditions that might produce a wider range of TNT layer dimensions on the 3D Ti meshes.

In summary, we demonstrated for the first time the photocatalytic application of additively manufactured 3D Ti meshes, modified with TNT layers by wireless anodization. It is believed that the large surface area of the TNT-layer-modified 3D Ti meshes will offer the key to a wide range of applications. In comparison to the classical 2D Ti substrates, the additive manufacturing of 3D meshes significantly enhances the surface area, which has a great advantage for applications such as photo- and electrocatalysis, sensing, and water splitting. Furthermore, the meshes have a great potential for self-supported flow-through catalytic systems. The application of bipolar electrochemistry facilitates the anodization of the 3D Ti meshes, as the establishment of any electrical contact on the Ti substrate is gratuitous.

METHODS

3D Ti meshes with a diameter of 20 mm and a height of 8 mm were fabricated by DIW.[10] The ink was prepared by mixing commercially pure spherical Ti powder (ASTM grade 1; TLS-Technik, Germany) with a particle size of 20−63 μm with an organic binder soluble in water, gelatin. The ink was introduced into the cartridge of the robotic deposition device immediately after mixing. Two different kinds of meshes were fabricated in air at a speed of 20 mm/s using an orthogonal deposition pattern in consecutive layers with the distances between filaments of 857 ± 26 and 1173 ± 56 μm, respectively. The porosity of the Ti meshes equals 68 ± 1% and 71 ± 1%, while the effective surface areas were 61 and 55 cm^2, which are equivalent to 2.4 and 2.2 mm^2/mm^3, respectively. The meshes were allowed to dry at room temperature for 12 h. Afterward, the binder was removed by heating in air to 350 °C for 12 h in a muffle furnace, and then the meshes were sintered under an argon atmosphere at 1400 °C for 10 h. After sintering the meshes had an equiaxial α-Ti grain microstructure free of secondary phases and visually showed a metallic aspect.

Before further use, the meshes were sonicated in isopropanol and acetone for 1 min each, rinsed with isopropanol, and dried in air.

Electrochemical anodization of the 3D Ti meshes was carried out in an ethylene glycol based electrolyte containing 170 mM NH_4F and 1.5 vol % of H_2O using bipolar electrochemistry.[9] For this, two Pt foils were used as feeder electrodes, connected to a high-voltage potentiostat (PGU-200V, IPS Elektroniklabor GmbH). The Ti meshes were

https://doi.org/10.1021/acs.nanolett.1c02815
Nano Lett. 2021, 21, 8701−8706

placed upright between the feeder electrodes with a distance of ~0.5 cm to both feeder electrodes. The anodization was carried out using an alternating potential of ±140 V for 4 h with frequencies of 0.0667, 0.0167, and 5.55×10^{-4} Hz, i.e. keeping the potential constant for 15 s, 60 s, or 30 min, respectively, before changing its direction. Before and during anodization the electrolyte was cooled to 5 °C.

TNT layers on Ti foils (Sigma-Aldrich, 127 μm thick) were prepared in the same electrolyte at 60 V for 4 h using a conventional anodization setup with a Ti foil as the anode and a Pt foil as the cathode.

After anodization the Ti meshes and foils were annealed in a muffle oven at 400 °C for 1 h at a heating rate of 2.1 °C/min and cooled naturally in order to obtain an anatase crystalline structure.

3D Ti meshes decorated with TiO_2 nanoparticles (NPs) were prepared using hydrolysis of $TiCl_4$.[32] $TiCl_4$ (Sigma-Aldrich, 99.9%) and deionized water were used for the preparation of a 1 M $TiCl_4$ solution at ~1−4 °C. The 3D Ti meshes were completely immersed into the pickling solution and ultrasonicated at room temperature for 15 s at 37 kHz with 50% power, followed by storage at 70 °C for 30 min and rinsing with deionized water. This chemical treatment was repeated four times and considered as four dips of NP decoration. Finally, the NP-decorated 3D Ti meshes were annealed at 400 °C for 1 h at a heating rate of 2.1 °C/min.

The morphology of the TNT layers was characterized using a field-emission scanning electron microscope (JEOL JSM 7500F). Cross-section images were obtained by carefully scratching the TNT layers from the Ti meshes. Proprietary Nanomeasure software was used to measure the nanotube diameter and the TNT layer thickness by analyzing a minimum of six SEM images for each anodization condition.

The XRD patterns for 3D Ti meshes and Ti foils were acquired on a Panalytical Empyrean diffractometer using a Bragg−Brentano geometry. The diffractometer was equipped with a Cu X-ray tube in point focus mode and a monocapillary of 135 mm length with a 0.1 mm diameter size output beam. The detector was Pixcel3D, working in scanning mode. The patterns were measured in the 2θ range of 5−65° with a step size of 0.026°.

Photocatalytic degradation of methylene blue (MB) dye was carried out in a homemade quartz glass reactor at room temperature. Six anodized and annealed 3D Ti meshes were stacked horizontally into the reactor, and 27 mL of a 1×10^{-5} M MB solution was added. Six nonanodized 3D Ti meshes with thermal oxide (annealed under the conditions described above) and six NP-decorated meshes were used as references. Prior to the photocatalytic measurements, the Ti meshes were kept in the MB solution for 1 h in the dark to reach an adsorption/desorption equilibrium of the dye. Afterward, the reactor was irradiated by an LED-based UV lamp (10 W, λ = 365 ± 5 nm, intensity 555 mW/cm^2) under constant stirring (170 rpm) of the MB solution, and the optical absorbance of the MB solution was periodically measured using a UV−vis spectrometer (S-200, Boeco) at a wavelength of 670 nm to monitor the dye degradation rates.

■ ASSOCIATED CONTENT

Supporting Information

The Supporting Information is available free of charge at https://pubs.acs.org/doi/10.1021/acs.nanolett.1c02815.

Additional SEM images of the TiO_2-nanoparticle-modified 3D Ti meshes before and after their use in photocatalysis and additional SEM images of the TNT-layer-modified 3D Ti meshes after their use for photocatalysis (PDF)

■ AUTHOR INFORMATION

Corresponding Author

Jan M. Macak − *Center of Materials and Nanotechnologies, Faculty of Chemical Technology, University of Pardubice, 53002 Pardubice, Czech Republic; Central European Institute of Technology, Brno University of Technology, 612 00 Brno, Czech Republic;* orcid.org/0000-0001-7091-3022; Email: jan.macak@upce.cz

Authors

Hanna Sopha − *Center of Materials and Nanotechnologies, Faculty of Chemical Technology, University of Pardubice, 53002 Pardubice, Czech Republic; Central European Institute of Technology, Brno University of Technology, 612 00 Brno, Czech Republic*

Adelia Kashimbetova − *Central European Institute of Technology, Brno University of Technology, 612 00 Brno, Czech Republic*

Ludek Hromadko − *Center of Materials and Nanotechnologies, Faculty of Chemical Technology, University of Pardubice, 53002 Pardubice, Czech Republic; Central European Institute of Technology, Brno University of Technology, 612 00 Brno, Czech Republic*

Ivan Saldan − *Central European Institute of Technology, Brno University of Technology, 612 00 Brno, Czech Republic*

Ladislav Celko − *Central European Institute of Technology, Brno University of Technology, 612 00 Brno, Czech Republic*

Edgar B. Montufar − *Central European Institute of Technology, Brno University of Technology, 612 00 Brno, Czech Republic*

Complete contact information is available at: https://pubs.acs.org/10.1021/acs.nanolett.1c02815

Author Contributions

H.S.: conceptualization, TNT layer synthesis, photocatalysis, data curation, scientific discussion, writing, and review of the manuscript. A.K.: 3D Ti mesh design, DIW and characterization of 3D Ti meshes, scientific discussion, and review of the manuscript. L.H.: SEM investigation and XRD analysis. I.S.: TiO_2 nanoparticle modification. L.C.: sintering, scientific discussion, funding acquisition, and review of the manuscript. E.B.M.: supervision, scientific discussion, funding acquisition, and review of the manuscript. J.M.M.: conceptualization, scientific discussion, funding acquisition, and review of the manuscript.

Notes

The authors declare no competing financial interest.

■ ACKNOWLEDGMENTS

The authors acknowledge the Ministry of Education, Youth and Sports of the Czech Republic (LM 2018103 and LTAIN19112) and the Czech Science Foundation (21-27243S). A.K. acknowledges the Brno Ph.D. Talent scholarship founded by the Brno City Municipality.

REFERENCES

(1) Macak, J. M.; Tsuchiya, H.; Ghicov, A.; Yasuda, K.; Hahn, R.; Bauer, S.; Schmuki, P. TiO2 Nanotubes: Self-Organized Electrochemical Formation, Properties and Applications. *Curr. Opin. Solid State Mater. Sci.* **2007**, *11* (1−2), 3−18.

(2) Lee, K.; Mazare, A.; Schmuki, P. One-Dimensional Titanium Dioxide Nanomaterials: Nanotubes. *Chem. Rev.* **2014**, *114* (19), 9385−9454.

(3) Liu, Z.; Subramania, V. R.; Misra, M. Vertically Oriented TiO2 Nanotube Arrays Grown on Ti Meshes for Flexible Dye-Sensitized Solar Cells. *J. Phys. Chem. C* **2009**, *113* (31), 14028−14033.

(4) Kapusta-Kołodziej, J.; Chudecka, A.; Sulka, G. D. 3D Nanoporous Titania Formed by Anodization as a Promising Photoelectrode Material. *J. Electroanal. Chem.* **2018**, *823*, 221−233.

(5) Martin, M.; Leonid, S.; Tomas, R.; Jan, S.; Jaroslav, K.; Mariana, K.; Michaela, J.; Frantisek, P.; Gustav, P. Anatase TiO2 Nanotube Arrays and Titania Films on Titanium Mesh for Photocatalytic NOX Removal and Water Cleaning. *Catal. Today* **2017**, *287*, 59−64.

(6) Gulati, K.; Santos, A.; Findlay, D.; Losic, D. Optimizing Anodization Conditions for the Growth of Titania Nanotubes on Curved Surfaces. *J. Phys. Chem. C* **2015**, *119* (28), 16033−16045.

(7) Yang, L.; Zheng, X.; Liu, M.; Luo, S.; Luo, Y.; Li, G. Fast Photoelectro-Reduction of Cr VI over MoS 2 @TiO 2 Nanotubes on Ti Wire. *J. Hazard. Mater.* **2017**, *329*, 230−240.

(8) Lashkov, A. V.; Fedorov, F. S.; Vasilkov, M. Y.; Kochetkov, A. V.; Belyaev, I. V.; Plugin, I. A.; Varezhnikov, A. S.; Filipenko, A. N.; Romanov, S. A.; Nasibulin, A. G.; Korotcenkov, G.; Sysoev, V. V. The Ti Wire Functionalized with Inherent TiO2 Nanotubes by Anodization as One-Electrode Gas Sensor: A Proof-of-Concept Study. *Sens. Actuators, B* **2020**, *306*, 127615.

(9) Sopha, H.; Hromadko, L.; Motola, M.; Macak, J. M. Fabrication of TiO2 Nanotubes on Ti Spheres Using Bipolar Electrochemistry. *Electrochem. Commun.* **2020**, *111*, 106669.

(10) Montufar, E. B.; Tkachenko, S.; Casas-Luna, M.; Škarvada, P.; Slámečka, K.; Diaz-de-la-Torre, S.; Koutný, D.; Paloušek, D.; Koledova, Z.; Hernández-Tapia, L.; Zikmund, T.; Čelko, L.; Kaiser, J. Benchmarking of Additive Manufacturing Technologies for Commercially-Pure-Titanium Bone-Tissue-Engineering Scaffolds: Processing-Microstructure-Property Relationship. *Addit. Manuf.* **2020**, *36* (July), 101516.

(11) Sopha, H.; Baudys, M.; Krbal, M.; Zazpe, R.; Prikryl, J.; Krysa, J.; Macak, J. M. Scaling up Anodic TiO2 Nanotube Layers for Gas Phase Photocatalysis. *Electrochem. Commun.* **2018**, *97*, 91−95.

(12) Zhao, P.; Liu, Y.; Li, T.; Zhou, Y.; Leeflang, S.; Chen, L.; Wu, C.; Zhou, J.; Huan, Z. 3D Printed Titanium Scaffolds with Ordered TiO2 Nanotubular Surface and Mesoporous Bioactive Glass for Bone Repair. *Prog. Nat. Sci.* **2020**, *30* (4), 502−509.

(13) Gulati, K.; Prideaux, M.; Kogawa, M.; Lima-Marques, L.; Atkins, G. J.; Findlay, D. M.; Losic, D. Anodized 3D-Printed Titanium Implants with Dual Micro- and Nano-Scale Topography Promote Interaction with Human Osteoblasts and Osteocyte-like Cells. *J. Tissue Eng. Regener. Med.* **2017**, *11* (12), 3313−3325.

(14) Maher, S.; Kaur, G.; Lima-Marques, L.; Evdokiou, A.; Losic, D. Engineering of Micro- to Nanostructured 3D-Printed Drug-Releasing Titanium Implants for Enhanced Osseointegration and Localized Delivery of Anticancer Drugs. *ACS Appl. Mater. Interfaces* **2017**, *9* (35), 29562−29570.

(15) Bose, S.; Banerjee, D.; Shivaram, A.; Tarafder, S.; Bandyopadhyay, A. Calcium Phosphate Coated 3D Printed Porous Titanium with Nanoscale Surface Modification for Orthopedic and Dental Applications. *Mater. Des.* **2018**, *151*, 102−112.

(16) Nune, K.; Misra, R.; Gai, X.; Li, S.; Hao, Y. Surface Nanotopography-Induced Favorable Modulation of Bioactivity and Osteoconductive Potential of Anodized 3D Printed Ti-6Al-4V Alloy Mesh Structure. *J. Biomater. Appl.* **2018**, *32* (8), 1032−1048.

(17) Qin, J.; Yang, D.; Maher, S.; Lima-Marques, L.; Zhou, Y.; Chen, Y.; Atkins, G. J.; Losic, D. Micro- and Nano-Structured 3D Printed Titanium Implants with a Hydroxyapatite Coating for Improved Osseointegration. *J. Mater. Chem. B* **2018**, *6* (19), 3136−3144.

(18) Wei, Y.; Hu, Y.; Li, M.; Li, D. Sr-Containing Micro/Nano-Hierarchical Textured TiO2 Nanotubes on 3D Printing Titanium. *Inorg. Chem. Commun.* **2020**, *117* (April), 107947.

(19) Ren, B.; Wan, Y.; Liu, C.; Wang, H.; Yu, M.; Zhang, X.; Huang, Y. Improved Osseointegration of 3D Printed Ti-6Al-4V Implant with a Hierarchical Micro/Nano Surface Topography: An in Vitro and in Vivo Study. *Mater. Sci. Eng., C* **2021**, *118*, 111505.

(20) Maher, S.; Wijenayaka, A. R.; Lima-Marques, L.; Yang, D.; Atkins, G. J.; Losic, D. Advancing of Additive-Manufactured Titanium Implants with Bioinspired Micro- to Nanotopographies. *ACS Biomater. Sci. Eng.* **2021**, *7* (2), 441−450.

(21) Lee, C.-Y.; Taylor, A. C.; Beirne, S.; Wallace, G. G. 3D-Printed Conical Arrays of TiO 2 Electrodes for Enhanced Photoelectrochemical Water Splitting. *Adv. Energy Mater.* **2017**, *7* (21), 1701060.

(22) Loget, G.; Schmuki, P. H2Mapping on Pt-Loaded TiO2 Nanotube Gradient Arrays. *Langmuir* **2014**, *30* (50), 15356−15363.

(23) Loget, G.; So, S.; Hahn, R.; Schmuki, P. Bipolar Anodization Enables the Fabrication of Controlled Arrays of TiO2 Nanotube Gradients. *J. Mater. Chem. A* **2014**, *2* (42), 17740−17745.

(24) Wei, W.; Björefors, F.; Nyholm, L. Hybrid Energy Storage Devices Based on Monolithic Electrodes Containing Well-Defined TiO2 Nanotube Size Gradients. *Electrochim. Acta* **2015**, *176*, 1393−1402.

(25) Li, Y.; Dong, Y.; Yang, Y.; Yu, P.; Zhang, Y.; Hu, J.; Li, T.; Zhang, X.; Liu, X.; Xu, Q.; Huang, Q.; Lin, C. Rational Design of Silver Gradient for Studying Size Effect of Silver Nanoparticles on Contact Killing. *ACS Biomater. Sci. Eng.* **2019**, *5* (2), 425−431.

(26) Mu, P.; Li, Y.; Zhang, Y.; Yang, Y.; Hu, R.; Zhao, X.; Huang, A.; Zhang, R.; Liu, X.; Huang, Q.; Lin, C. High-Throughput Screening of Rat Mesenchymal Stem Cell Behavior on Gradient TiO 2 Nanotubes. *ACS Biomater. Sci. Eng.* **2018**, *4* (8), 2804−2814.

(27) Saqib, M.; Lai, J.; Zhao, J.; Li, S.; Xu, G. Bipolar Electrochemical Approach with a Thin Layer of Supporting Electrolyte towards the Growth of Self-Organizing TiO 2 Nanotubes. *ChemElectroChem* **2016**, *3* (3), 360−365.

(28) Macak, J. M.; Albu, S. P.; Schmuki, P. Towards Ideal Hexagonal Self-Ordering of TiO2 Nanotubes. *Phys. Status Solidi RRL* **2007**, *1* (5), 181−183.

(29) Sopha, H.; Jäger, A.; Knotek, P.; Tesař, K.; Jarosova, M.; Macak, J. M. Self-Organized Anodic TiO2 Nanotube Layers: Influence of the Ti Substrate on Nanotube Growth and Dimensions. *Electrochim. Acta* **2016**, *190*, 744−752.

(30) Albella, J. M.; Montero, I.; Martinez-Duart, J. M. A Theory of Avalanche Breakdown during Anodic Oxidation. *Electrochim. Acta* **1987**, *32* (2), 255−258.

(31) Alijani, M.; Sopha, H.; Ng, S.; Macak, J. M. High Aspect Ratio TiO2 Nanotube Layers Obtained in a Very Short Anodization Time. *Electrochim. Acta* **2021**, *376*, 138080.

(32) Sopha, H.; Krbal, M.; Ng, S.; Prikryl, J.; Zazpe, R.; Yam, F. K.; Macak, J. M. Highly Efficient Photoelectrochemical and Photocatalytic Anodic TiO_2 Nanotube Layers with Additional TiO_2 Coating. *Appl. Mater. Today* **2017**, *9*, 104−110.

https://doi.org/10.1021/acs.nanolett.1c02815
Nano Lett. 2021, 21, 8701−8706